Optimal Scheduling of Multi-Carrier Energy Hubs with Demand Response and Electric Vehicles for Cost Reduction and Flexibility Enhancement

Shaimaa A. M. Mousa[1, □], Abdelfatah Ali[1], Karar Mahmoud[2], and Essam E. M. Mohamed[1]

Abstract Worldwide, energy hubs (EHs) have been developed by integrating different technologies for power transformation, storage, and generation, as a critical key to overcoming resource insufficiency and environmental issues. Moreover, the energy center performs a major task by enhancing system flexibility, efficiency, and reliability. The attention to electric vehicles (EVs) and renewable energies has also increased. An EH consists of combined cooling, heating, and power (CCHP) units, wind turbines (WTs), photovoltaics (PVs), hydrogen electrolyzers, fuel cells (FCs), water desalination systems, auxiliary boilers (AB), plug-in electric vehicles (PEVs) and energy storage systems (ESSs); ice storage conditioners (ISCs), solar powered compressed air energy storage (SPCAES), thermal energy storage systems (TESSs), hydrogen storage (H2S). This paper employs a demand response program (DRP), for load curtailment, shifting, and flexible load modeling. In pursuit of reducing the total costs. Herein, four scheduling cases are evaluated using different charging modes of EVs and applying the DRP. The numerical results reveal that, by implementing the electrical DRP (EDRP), the final costs are successfully reduced. Compared to the base case, the total costs are reduced by 4.0% when the EDRP is applied. The total costs decreased by 4.8% when both electrical and thermal DRPs were employed. The results also demonstrate that by implementing both DRPs and coordinated mode EVs, total costs can be further decreased by 6.3%.

Keywords: (energy hub; demand response program; hydrogen system; electric vehicles; sea water desalination).

1. Introduction

Due to population increase, rapid developments in the field of economics, technological progress, and technical development in recent decades, there has been a clear increase in global demand for energy [1, 2]. Owing to the increase in energy demand, traditional energy systems based on fossil fuels have also increased, and therefore there has been a significant increase in energy prices and emissions [3-5]. Moreover, separate management of energy resources and systems increases operating costs and emissions while reducing system efficiency [6]. Therefore, various aspects of the concept of sustainable energy have been studied so far. To get maximum profit from the existing energy resources, different power resources have been used and scheduled in the form of a multi-power network [7-9]. Therefore, EHs are energy systems that directly connect several energy carriers such as electricity, heat, gas, and hydrogen. The ability to store, transport, and convert various energy carriers acts as an interface between consumers and producers [9-12].

To highlight the advantages of energy hub (EH), combined heat and power (CHP) and combined cooling, heat and power (CCHP) modules are used [13]. One of the key characteristics of EHs is their ability to be implemented for different sizes of power systems. Therefore, it can be used for residential power centers [14, 15]. Moreover, the fundamental needs for zero-emission energy generation make renewable energy sources more significant than ever [16]. In addition, The use of renewable energy resources (RES) in EHs improves the environmental features of the power system and reduces the operating cost because its

□Corresponding Author: **Shaimaa A. M. Mousa**,
sha.abdelhameed@gmail.com.
1. Department of Electrical Engineering, South Valley University, 83523 Qena, Egypt.
2. Department of Electrical Engineering, Aswan University, 81542 Aswan, Egypt.

operating and maintenance costs are not high [4]. Although it does not have deterministic outcomes due to the unpredictable nature of its primary sources. These uncertainties related to renewable energy systems, along with uncertainties related to energy demand, lead to more challenges facing the energy center. Looking at the worst-case scenario is a solution that requires paying huge costs [17]. In addition, the appropriate alternative for increasing the efficiency of the system and overcoming uncertainties is the use of energy storage systems (ESS). Implementing RES such as photovoltaic (PV) modules, and wind turbines (WTs), in addition to the storage systems which include electrical storage systems (ESSs), thermal storage facilities, natural gas (NG) storage systems, and gas power plant is the proposed EH in ref [18]. In addition, the output power uncertainty of WT and PV units was considered using a genetic algorithm (GA). A new stochastic model for different uncertainties in EHs, such as REDRs, load, electricity price, and output power was studied in ref [19]. A Robust Mixed Integer Linear Programming (RMILP) approach was used to consider the uncertainty related to the RES, loads, the energy required for charging the (EVs) and electricity price [20].

Due to the increasing growth in energy demand in recent years, the use of demand response programs (DRPs) has become widely spread as a suitable alternative to fix load curves and increase system efficiency. For alleviating the EH drawbacks, the integration of DRP effectively contributes to improving the EH operation as in [21, 22] which presents a 13.78% improvement in the total costs of the EH system. In addition, DRP was integrated to improve both aspects of the operation and reliability of the EH in ref [23]. Ignoring the effects of uncertainty in [24, 25] the EH model in ref [25] is integrated with energy storage, DRP, and RESs such as WT and PV cells. To reduce operational and environmental costs under mixed integer linear programming (MILP) a scenario-based stochastic process for EH integrated with solar-powered compressed air energy storage (SPCAES) and ice storage conditioner (ISC) is illustrated in ref [26] which improves the total cost by 2.6% by combining the ISC and the SPCAES. Electric DRP was used to develop energy management of EH in ref [27], Which improves the operating costs by 24% in the presence of ice storage though electric vehicles (EVs) have not been considered. For managing loads in different periods, real-time DRP has been used while the main component of the EH was the CCHP. However, the uncertain nature of RESs and EVs was not taken into account in ref [28] and the cost reduction is up to 5.2% due to the employment of DRP.

For managing large-scale resources and considering uncertainties related to EVs, market prices, and RES output power, a stochastic model was proposed in ref [29]. Various uncertainties of power systems in the presence of EVs were investigated, although the heating and cooling loads were not studied in ref [30]. Depending on load classifications, ref [31] has examined the integrated DRP. By integrating electrical and thermal DRP a robust optimization process for managing EHs was investigated in ref [32]. Owing to the widespread use of hydrogen as a clean fuel[33, 34], [35] a robust integrated DRP-based optimization method for EHs that incorporates the hydrogen system which includes fuel cells (FCs) and hydrogen storage (H2S) systems with a decrement in the operating costs up to 7.8%. Due to the scarcity of fresh water in many areas around the world, getting clean water has become an increasingly important problem [36]. As a consequence, 25% of the world's population cannot obtain a sufficient amount of freshwater [37]. Therefore, to obtain fresh water, specifically in coastal regions seawater desalination (SWD) processes have been commonly integrated into energy centers (EHs) [38]. Due to the need to provide reliable sources of clean fresh water for various uses to human communities in areas facing the problem of water shortage, SWD's reverse osmosis (RO) technology draws attention due to its economic performance [39]. The use of CCHP and renewable generations in combination with grid-connected and islanded microgrids (MGs) based on EH with the SWDs regarding several studies were done [40, 41].

The literature review shows that there are two principal research gaps, namely considering the demand for pure water, hydrogen, and EVs, along with implementing electrical and thermal DRP for the robust optimization of EHs. This paper attempts to fill these research gaps. In the proposed robust optimization method, all the EH loads including electrical, thermal, cooling as well as hydrogen and pure water demand are taken into account, which is one of the main contributions of this study. Studying the effects of different hybrid ESSs, including SPCAES, thermal energy storage systems (TESS), ISC, and H2S, is another advantage of the proposed method. The integrated thermal and electrical DRPs were also studied. Moreover, the effects of uncoordinated and coordinated charging modes of EVs were characterized in this study.

Table 1. The summary of the literature review and the comparison of the proposed method with other works

		Loads					Storages							DRP	
Ref	Year	Electrical	Thermal	Cooling	Hydrogen	Water	ES	HS	CS	H2S	PV	WT	EVs	EDRP	HDRP
[23]	2014	√	√	-	-	-	√	√	-	-	-	√	-	√	-
[42]	2015	√	√	-	-	-	-	√	-	-	√	√	-	-	-
[13]	2017	√	√	√	-	-	-	-	-	-	√	√	-	-	-
[43]	2017	√	√	√	-	-	√	√	√	-	√	√	-	√	-
[44]	2018	√	-	-	-	-	-	-	-	-	√	√	√	-	-
[25]	2019	√	√	√	-	-	√	√	-	-	-	-	-	-	-
[45]	2019	√	√	√	-	-	√	√	√	-	-	-	√	√	-
[46]	2019	√	√	√	-	-	√	√	√	-	√	√	-	√	√
[14]	2020	√	√		-	-	√	√	-	-		√	-	√	√
[18]	2020	√	√	√	-	-	√	√	√	-	√	√	-	-	-
[47]	2020	√	√	-	-	-		√	-	-	√	√	√	√	√
[48]	2021	√	√	√	-	-	√	√	√	-	√	-	-	√	√
[49]	2021	√	√	√	-	-	√	√	-	-		√	-	√	√
[15]	2021	√	√	-	-	-	-	√	-	-	√	-	√	-	-
[50]	2022	√	√	√	√	√		√	√	√	√	√	√	-	-
[30]	2022	√	√	√	-	-	√	-	-	-	√	√	√	√	-
[11]	2023	√	√	√	√		√	√	√	√	√	√	√	√	√
Proposed method		√	√	√	√	√	√	√	√	√	√	√	√	√	√

The innovative characteristics and the main contributions of this study can be summarized as follows:

- Due to the rapid spread of electric vehicles recently several references studied the optimal operation of EHs with considering EVs. However, there is a gap in studying the impacts of EVs and their charging modes on the optimal operation of EH. Therefore, studying the effects of EVs and their managed and unmanaged charging modes is one of the main contributions of this paper.
- The effects and advantages of different storage systems including ISC, TESS, H2S, and SPCAES on the optimal EH performance during EVs' charging mode in different seasons are also included.
- To provide fresh water for the regions facing the water inadequacy problem, SWD-RO should be heavily investigated. The hydrogen system is also included to provide clean fuel. Therefore, this study has focused on the hydrogen and freshwater demands, which did not receive the required attention in existing studies.
- Most published studies don't provide a detailed analysis of the effect of electrical/thermal/integrated

electrical and thermal DRP on the EH optimal operation which is an essential contribution of this article compared to existing studies.

The proposed energy management scheme takes into account electricity, heat, cooling, hydrogen, and purified water requirements simultaneously, along with integrated electrical and thermal DRP. Considering the different requirements and supplying them to EH through the use of different generating units and ESSs is one of the strengths of this article. **Table 1** produces the summary of the literature review and the comparison of the proposed method with other works.

Following are the sections of the study: Section 2 introduces the EH configuration. Section 3 presents the proposed model for the optimal EH operation. The uncertainty modeling is described in Section 4. Part 5 discusses the mathematical model and solution algorithm. Part 6 discusses simulation results and discussions. Finally, the conclusion is reported in Section 7.
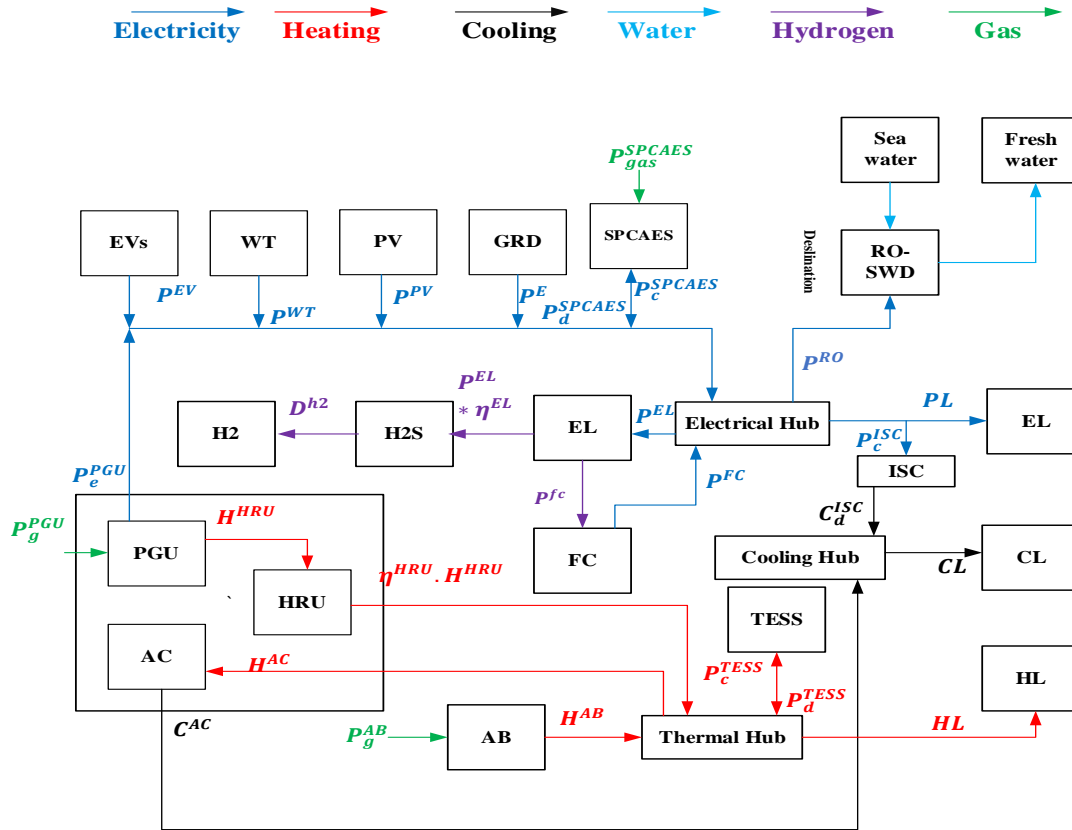
Fig 1. The proposed EH architecture.

2. EH configuration

The intermediate connection in the energy supply chain between primary resources and the ultimate customers are energy carriers, which include electricity and heat, besides other solid, liquid, and gaseous fuels. Moreover, an energy system that includes more than one energy carrier is represented as a multi-carrier energy system or energy center. Whereas, EH can be represented as a node through which different energy carriers such as heat, electricity, and cooling are transformed to each other by different energy converters. Furthermore, the EH also contains an energy storage, transmission, and distribution system.

This section focuses on explaining and formulating the elements of EH. As shown in **Fig. 1**, the EH system consists of CCHP, WT, PV, SPCAES, AB, absorption chiller (AC), EVs, TESS, ISC, water desalination system-based RO technology, and hydrogen system. The CCHP consists of several components such as a power generation unit (PGU), heat recovery unit (HRU), and AC. The PGU consumes NG

for generating electricity, and excess heat is captured by the HRU to reduce waste. AB works alongside HRU as another heat generator, generating thermal energy through NG consumption. The heat from the thermal hub serves as an input for the AC for cool production. While ISC also contributes to providing cooling requirements [4] relieving pressure on the power supply and achieving a balance within the cooling hub between generation and demand. In addition, the integration of TESS enhances the overall reliability of the power system. Moreover, it is preferable to use SPCAES over traditional compressed air energy storage (CAES), as higher efficiency is obtained through it. Despite their obvious similarity, SPCAES collects the output of the solar collector along with the heat recuperator.

As illustrated in **Fig. 1**, the inputs to the EH can be obtained from both electrical and NG networks, while the loads include electricity, heat, cooling, pure water, and hydrogen. Also, the electrical hub is supplied with electrical energy via the utility grid, PV, WT, FC, and the electrical energy generated by the CCHP. In addition, the SPCAES exchanges the electrical energy with the electrical hub. The electric hub must meet the requirements of the electric load,

the energy consumed by the electrolyzer, the energy consumed by the water desalination system, and the charging load of EVs. It should be noted that EVs can be charged through a coordinated/uncoordinated charging system, which is studied in this paper, along with integrated thermal and electrical DRP systems. As for the cooling loads, they are provided through a cooling center through AC and ISC. Moreover, the heat requirement of the heating hub is provided by the AB and HRU; the heat storage can also be charged or discharged at required times. The SWD system uses RO technology, through which water is generated using electrical energy to meet the demand for fresh water. To get the required balance between hydrogen production and utilization, the electrolyzers, a hydrogen tank, along with FC are implemented.

3 The proposed model for optimal EH operation

3.1. Objective function and energy balance constraints:

3.1.1 Objective function:

As discussed, the main purpose of this study is to reduce the total costs of the proposed model, which includes the operating costs and environmental costs, besides reducing the consumers' discomfort cost related to integrating electrical and thermal DRP.

Eq. (1) details the total costs of EH. Firstly, operating costs are costs related to energy and gas purchased from the electricity and gas markets as formulated in Eqs. (2-3) respectively.

$$C_{TOT} = \min (C_e + C_g + C_{ce} + C_{EDRP} + C_{HDRP}) \qquad (1)$$

$$C_e = \sum_{t=1}^{N_t} (\rho_e(t). P^{Grid}. \Delta t) \qquad (2)$$

$$C_g = \sum_{t=1}^{N_t} (\rho_g(t). \left[\frac{P_e^{PGU}(t)}{\eta_e^{PGU}} + \frac{H^{HRU}(t)}{\eta_h^{PGU}} + \frac{H^{AB}(t)}{\eta_h^{AB}} + \frac{P_d^{SPCAES}(t)}{\eta_d^{SPCAES}} \right]). \Delta t) \qquad (3)$$

Where, C_{TOT} is the total cost of EH, C_e is the net electricity purchasing cost, C_g is the net gas purchasing cost, C_{ce} is the carbon emission cost, C_{EDRP} and C_{HDRP} are the discomfort costs resulting from implementing electrical and thermal DRP respectively, ρ_e is the Sell and purchase Electricity price, P^{Grid} is the real power exchanged from the upstream grid, ρ_g is the gas price, θ is the carbon dioxide processing cost, Φ_e is the equivalent emission coefficient for electricity, and Φ_g is the equivalent emission coefficient for natural gas.

As shown in (3), the amount of NG withdrawn from the NG network is consumed through the SPCAES during the generating mode, PGU and AB together. The cost of processing emissions resulting from supplying various loads with energy through non-renewable energy conversion methods, such as CCHP units and boilers, is calculated based on electricity purchased from the network and the amount of NG withdrawn from the NG network using (4).

$$C_{ce} = \sum_{t=1}^{N_t} \theta \left(\Phi_e. P^{Grid}(t) + \Phi_g. \left[\frac{P_e^{PGU}(t)}{\eta_e^{PGU}} + \frac{H^{HRU}(t)}{\eta_h^{PGU}} + \frac{H^{AB}(t)}{\eta_h^{AB}} + \frac{P_d^{SPCAES}(t)}{\eta_d^{SPCAES}} \right] \right). \Delta t \qquad (4)$$

Moreover, the cost of customers' dissatisfaction resulting from integrated thermal and electrical DRPs is mainly because they have to change their energy consumption pattern versus their comfort standards while participating in DRP[51]. Therefore, the dissatisfaction costs arising from electrical and thermal DRPs should be defined by (5) and (6), respectively.

$$C_{EDRP} = \sum_t P^{UP}(t) \times \emptyset^{E,UP} + P^{DO}(t) \times \emptyset^{E,DO} \qquad (5)$$

$$C_{HDRP} = \sum_t H^{UP}(t) \times \emptyset^{H,UP} + H^{DO}(t) \times \emptyset^{H,DO} \qquad (6)$$

3.1.2 Energy balance constraints:

The electrical hub power balance can be written as:

$$
\begin{aligned}
P^E(t) + P^{PV}(t) + P^{WT}(t) + P_e^{PGU}(t) + \\
P_d^{SPCAES}(t) + P^{FC}(t) + P^{DO}(t) = \\
PL(t) + P^{EV}(t) + P_c^{ISC}(t) + \\
P_c^{SPCAES}(t) + P^{EL}(t) + \\
P^{RO}(t) + P^{UP}(t)
\end{aligned} \qquad (7)
$$

Furthermore, the thermal hub power balance is illustrated as:

$$
\begin{aligned}
\eta^{HRU}. H^{HRU}(t) + H^{AB}(t) + P_d^{TESS}(t) + H^{DO}(t) = \\
HL(t) + H^{AC} + P_c^{TESS}(t) + H^{UP}(t)
\end{aligned} \qquad (8)
$$

Moreover, the cooling hub energy balance is expressed as follows:

$$C^{AC}(t) + P_d^{ISC}(t) = CL(t) \qquad (9)$$

3.2 Modelling of equipment and constraints:

3.2.1 Modelling of hydrogen system:

At a given time, based on the hydrogen demand (D^{h2}) and FC hydrogen demand, the total hydrogen energy generated by the electrolyzer may or may not be sufficient to provide the total hydrogen energy demanded Therefore, H2S charges and discharges to reach the required balance between hydrogen generation and demand at each time segment as follows.

$$P^{EL}(t) \times \eta^{EL} = D^{h2}(t) + P^{fc}(t) + H2^{im}(t) - H2^{ex}(t) \quad \forall t \in T \tag{10}$$

Accordingly, the state of charge (SOC) of the H2S which represents the amount of hydrogen energy stored in H2S at each time segment can be calculated through the amount of hydrogen energy imported or exported from it, in addition to the amount of hydrogen stored in the H2S in the previous hour as the equations below.

$$SOC^{H2S}(t) = SOC^{H2S}(t-1) + \frac{H2^{im}}{HHV^{H2}} - \frac{H2^{ex}}{HHV^{H2}} \quad \forall t > 1 \tag{11}$$

$$SOC^{H2S}(t) = SOC_{ini}^{H2S} + \frac{H2^{im}}{HHV^{H2}} - \frac{H2^{ex}}{HHV^{H2}} \quad \exists t = 1 \tag{12}$$

The FC is used to supply the required electrical energy when the hydrogen energy is redundant and also when the electrical demand is at peak as in the following equation.

$$P^{FC} = P^{fc}(t) \times \eta^{FC} \qquad \forall t \in T \tag{13}$$

The restrictions related to the H2S are illustrated as:

$$U_c^{H2S}(t) + U_d^{H2S}(t) \leq 1 \quad \forall t \in T \tag{14}$$

$$H2^{im}(t) \leq U_c^{H2}(t) \times K \quad \forall t \in T \tag{15}$$

$$H2^{ex}(t) \leq U_d^{H2}(t) \times K \quad \forall t \in T \tag{16}$$

$$P^{EL}(t) \leq P^{EL-max} \qquad \forall t \in T \tag{17}$$

$$SOC^{H2S}(t) \leq SOC^{H2S-max} \quad \forall t \in T \tag{18}$$

As specified in (14) the H2S can't operate at the generating and load mode simultaneously. Eqs. (15-18) declares the corresponding limitations of the H2S and electrolyzer.

3.2.2 Reverse osmosis desalination unit modeling:

The interrelationships between freshwater generation and electricity consumption can be illustrated as follows:

$$P^{RO}(t) = W^{RO}(t) \times SEC^{RO} \tag{19}$$

Eq. 20 shows the correlation between the hourly freshwater demand and the amount of freshwater generated by the SWD unit. As shown, the amount of pure water produced from SWD is equal to the amount of water required every hour due to the absence of a water storage tank (WST).

$$W^{RO}(t) = W^{wd}(t) \tag{20}$$

3.2.3 Network modelling:

Through the transformer, electrical energy is exchanged between the network and the electrical hub. If electricity is in excess, EH exchanges the excess electricity with the utility grid. Nevertheless, when electricity is inadequate, EH purchases electricity from the grid as specified.

$$P^E = P^{Grid} \times \eta_t \tag{21}$$

In addition, constraint (22) indicates the allowable range of the electrical energy swapped between the EH and the grid.

$$P_{min}^E \leq P^E \leq P_{max}^E \tag{22}$$

3.2.4 CCHP unit modelling:

The CCHP units are basic energy-saving- facilities, which are fed with NG to produce electricity, cool, and heat simultaneously. As shown in Fig. 1, NG energy is consumed by the PGU (P_g^{PGU}) for producing electricity ($\boldsymbol{P_e^{PGU}}$) and co-product heat ($\boldsymbol{H^{HRU}}$) as illustrated by Eqs. (23) and (24).

$$P_e^{PGU} = P_g^{PGU} \times \eta_e^{PGU} \tag{23}$$

$$H^{HRU} = P_g^{PGU} \times \eta_h^{PGU} \tag{24}$$

The co-product heat produced by the PGU (H^{HRU}) acts as an input to the HRU and its output ($H^{HRU} \times \eta^{HRU}$) is injected into the thermal hub. Then the AC consumes part of the heat coming out of the thermal hub for generating cooling energy, which can be represented by the following equation:

$$C^{AC} = H^{AC} \times k^{AC} \tag{25}$$

The restrictions related to the minimum and maximum limits of the PGU, HRU, and AC are specified in Eqs (26)(27), and (28) respectively.

$$P_{min}^{PGU} \leq P_e^{PGU} \leq P_{max}^{PGU} \qquad (26)$$

$$H_{min}^{HRU} \leq H^{HRU} \leq H_{max}^{HRU} \qquad (27)$$

$$H_{min}^{AC} \leq H^{AC} \leq H_{max}^{AC} \qquad (28)$$

3.2.5 Storage modeling
A) SPCAES modeling

The SPCAES consumes NG during discharging periods, hence the SPCAES discharging equation is illustrated in Eq (29). In the case of charging, the SPCAES only consumes electrical energy working at the load mode.

$$P_d^{SPCAES} = P_{gas}^{SPCAES} \times \eta_d^{SPCAES} \qquad (29)$$

B) ISC modelling

The ISC is utilized in combination with the AC to get the required cooling energy in the EH. Therefore, the use of ISC offers many advantages, as it consumes electricity at off-peak times to produce cooling energy, hence shifting the electricity consumption from peak hours to off-peak hours, which reduces power supply tension, as formulated:

$$P_d^{ISC} = P_C^{ISC} \times k^{ISC} \qquad (30)$$

C) TESS modelling

TESS is ideally combined with other heating facilities, such as CCHP and AB units to meet the heating requirements of AC as well as the required heat loads. The TESS charges during off-peak times working at the load mode and discharges during on-peak times working in the generating mode. Thereby reducing the total cost.

D) Storages constraints

The SPCAES, TESS, and ISC constraints on the minimum/maximum charge/discharge energy and so on, are provided in a set of Eqs. (31) to (35).

$$0 \leq P_c^{ESS}(t) \leq P_{c-max}^{ESS} \times U^{ESS}(t) \qquad (31)$$

$$0 \leq P_d^{ESS}(t) \leq P_{d-max}^{ESS} \times (1 - U^{ESS}(t)) \qquad (32)$$

$$E^{ESS}(t) = E^{ESS}(t-1) - P_{d-max}^{ESS}(t) \times \eta_d^{ESS} + \left(\frac{P_{c-max}^{ESS}(t)}{\eta_c^{ESS}} \right) \qquad (33)$$

$$E_{min}^{ESS} \leq E^{ESS}(t) \leq E_{max}^{ESS} \qquad (34)$$

$$E^{ESS}(0) = E^{ESS}(24) \qquad (35)$$

3.2.6 Auxiliary boiler model

To serve heating customers, in addition to CCHP and TESS, AB is implemented as a common thermal product technology for producing thermal energy through the consumption of NG as follows:

$$H^{AB} = P_g^{AB} \times \eta_h^{AB} \qquad (36)$$

Moreover, the amount of thermal energy produced by the AB in each period must be within the minimum and maximum limits specified in Eq. (37).

$$H_{min}^{AB} \leq H^{AB} \leq H_{max}^{AB} \qquad (37)$$

3.2.7 EVs modeling

EVs charging model:
Because the behaviors of EV owners are random, for example, arrival time, departure time, and travel distance/tim[8] . A suitable probability distribution function (PDF) must be used to model the analytical behaviors of EV owners.

- EVs driving distance

$$F_D(X) = \frac{1}{\sqrt{2\pi}\sigma_D X} \exp \left(\frac{-(\ln X - \mu_D)^2}{2\sigma_D^2} \right) \qquad (38)$$

Eq. (38) declares the logarithmic distribution function of the daily EV driving distance.

- EVs' arrival and departure time

Charging of EVs usually begins in the evening when car owners arrive home. Through the normal distribution function, the arrival time of the electric vehicle is determined as formulated by Eq. (39).

$$F_{AR}(t)$$
$$= \begin{cases} \dfrac{1}{\sqrt{2\pi}\sigma_{AR}}\exp\left(\dfrac{-(t+24-\mu_{AR})^2}{2\sigma_{AR}^2}\right) & 0 \le t \le \mu_{AR}-12 \\[2mm] \dfrac{1}{\sqrt{2\pi}\sigma_{AR}}\exp\left(\dfrac{-(t-\mu_{AR})^2}{2\sigma_{AR}^2}\right) & \mu_{AR}-12 \le t \le 24 \end{cases} \tag{39}$$

Moreover, the departure time also follows normal distribution, as presented in Eq (40).

$$F_{DP}(t)$$
$$= \begin{cases} \dfrac{1}{\sqrt{2\pi}\sigma_{DP}}\exp\left(\dfrac{-(t-\mu_{DP})^2}{2\sigma_{DP}^2}\right) & 0 \le t \le \mu_{DP}+12 \\[2mm] \dfrac{1}{\sqrt{2\pi}\sigma_{DP}}\exp\left(\dfrac{-(t-24-\mu_{DP})^2}{2\sigma_{DP}^2}\right) & \mu_{DP}+12 \le t \le 24 \end{cases} \tag{40}$$

Furthermore, two popular EV charging modes affect EH operation significantly.

A) Uncoordinated EV charging mode:

The charging of the EVs in the uncoordinated mode depends on traveling distance, arrival time, departure time, and other EV characteristics.

B) Coordinated EV charging mode:

In this mode, the EVs on the contrary charge at off-peak hours simultaneously.

C) EVs constraints

$$E_{n,t}^{EV} = E_{n,t-1}^{EV} + \eta_{ch,n,t}^{EV} \times E_{ch,n,t}^{EV} \times \Delta t \\ - (\Delta t \times E_{dch,n,t}^{EV})/\eta_{dch,n,t}^{EV} \tag{41}$$

$$E_{min,n}^{EV} \le E_{n,t}^{EV} \le E_{max,n}^{EV} \tag{42}$$

$$0 \le E_{ch,n,t}^{EV} \le E_{ch-max,n}^{EV} \times \varepsilon_{ch,n,t}^{EV} \tag{43}$$

$$0 \le E_{dch,n,t}^{EV} \le E_{dch-max,n}^{EV} \times \varepsilon_{dch,n,t}^{EV} \tag{44}$$

$$\varepsilon_{ch,n,t}^{EV} + \varepsilon_{dch,n,t}^{EV} = 1, \forall n, t \in [t_{AR,n}, t_{DP,n}] \tag{45}$$

$$\varepsilon_{ch,n,t}^{EV} + \varepsilon_{dch,n,t}^{EV} = 0, \forall n, t\, [t_{AR,n}, t_{DP,n}] \tag{46}$$

$$0 \le \sum_n E_{ch,n,t}^{EV} \le E_{ch-max}^{EV} \tag{47}$$

$$0 \le \sum_n E_{dch,n,t}^{EV} \le E_{dch-max}^{EV} \tag{48}$$

As reflected in Eq. (41), the amount of energy stored in electric vehicle batteries is determined depending on the stored energy available in the previous time interval and the last discharge/charge energy. As in Eq. (42), The stored

energy must be limited to a certain range to protect the EVs' batteries. The peak value of charging and discharging energy of EVs are restricted as in Eqs. (43) and (44). Eq. (45) declares that when the EVs are associated with the EH, they cannot be charged and discharged simultaneously. However, if the EVs are not linked with the EH, they cannot be charged or discharged, which is restricted by Eq. (46). When EVs are charging or discharging, the maximum power transferred between the EVs and the EH in both cases is limited by Eqs. (47) and (48) respectively.

3.2.7 DRP model for Electrical and thermal loads

There are two distinct models of DRPs; price-based DRPs [52] and incentive-based [53]. In this paper, price-based DRP is considered. Thus, the proposed optimization problem should be solved, taking into consideration the thermal and electrical DRP limitations.

A. Electrical DRP limitations

The constraints of the electrical demand response program (EDRP) are as follows:

$$\sum_t P^{UP}(t) = \sum_t P^{DO}(t) \tag{49}$$

The total electrical power transferred upward must be equal to the electrical power transferred downward during each day of the study period (4 days) as in Eq. (49). The maximum amount of electrical energy shifted up/down is limited by the Eqs. (50) and (51) appropriately. The EDRP can't shift the electrical load up and down at the same time as illustrated by Eq. (52).

$$0 \le P^{UP}(t) \le (MR^{E,UP} \cdot PL(t) \cdot \varepsilon^{E,UP}(t)) \tag{50}$$
$$0 \le P^{DO}(t) \le (MR^{E,DO} \cdot PL(t) \cdot \varepsilon^{E,DO}(t)) \tag{51}$$
$$0 \le \varepsilon^{E,UP}(t) + \varepsilon^{E,DO}(t) \le 1 \tag{52}$$

In the above equations, $\varepsilon^{E,UP}(t)$ and $\varepsilon^{E,DO}(t)$ represents the logical variable of Shifting up/down of the electrical demand in period t. For example, the one value of $\varepsilon^{E,UP}(t)$ represents that the electrical demand is shifted up at the *t-th* interval. Otherwise, the zero value represents no shifting-up demand.

B) Thermal DRP limitations

As in the EDRP, the thermal demand response program (HDRP) decreases and increases the thermal load at certain

times according to the following restrictions:

$$\sum_t H^{UP}(t) = \sum_t H^{DO}(t) \qquad (53)$$
$$0 \le H^{UP}(t) \le (MR^{H,UP} * HL(t) * \varepsilon^{H,UP}(t)) \qquad (54)$$
$$0 \le H^{DO}(t) \le (MR^{H,DO} * HL(t) * \varepsilon^{H,DO}(t)) \qquad (55)$$
$$0 \le \varepsilon^{H,UP}(t) + \varepsilon^{H,DO}(t) \le 1 \qquad (56)$$

Eq. (53) illustrates that the total thermal energy transformed up should be equal to the thermal energy transformed down during each day of the study period. In addition, there are additional constraints on HDRP, as shown in Eq. (54-56).

4 Uncertainty modelling:

4.1 Wind power model

Because the energy generated from the wind system corresponds to the relevant wind speed. Therefore, WT power is calculated as in Eq. (57) implementing a Weibull PDF for modeling the uncertainty related to the stochastic performance of wind speed as indicated by Eq. (58)

$$p_w(v) = \begin{cases} 0 & 0 \le v \le v_{ci} \\ p_{rated} \times \dfrac{(v - v_{ci})}{(v_r - v_{ci})} & v_{ci} \le v \le v_r \\ p_{rated} & v_r \le v \le v_{co} \\ 0 & v_{co} \le v \end{cases} \qquad (57)$$

$$f_w(v) = ba^{-b}v^{b-1}e^{-(\frac{x}{a})^b} \qquad (58)$$

4.2 PV model

For modeling the solar irradiation of PV panels, a Beta PDF is used. Hence, The PDF of solar radiation (PDF) at any given hour is usually justified by a bimodal distribution function that linearly combines the two monomodal distributions with the beta PDF. For each unimodal distribution, the Beta PDF is used indicated by Eqs (59-61). Both the PV panel's output power and the power generated by the solar collector are a function of the efficiency of the PV modules, irradiance, and surface area which can be formulated by Eqs (62-63).

$$p_{pv}(si) = \eta^{pv} \times s^{pv} \times si \qquad (62)$$

$$p_{solar}(si) = \eta^{sol} \times s^{sol} \times si \qquad (63)$$

4.3 Loads uncertainty modeling

To model the uncertainty of all the requirements involved, which include hydrogen, cooling and heating, fresh water, and electricity, a normal PDF is used as shown.

$$f_d(l) = \frac{1}{\sigma_d \times \sqrt{2\pi}} \times e^{\frac{-(1-\mu_d)^2}{2\sigma_d^2}} \qquad (64)$$

$$l = z \times \sigma_d + \mu_d$$

5. Mathematical model and solution algorithm

5.1. PSO algorithm:

For continuous optimization problems, the standard particle swarm optimizer (PSO) algorithm is used as a kind of practical optimization method. PSO has many advantages such as low search rate and high convergence. Therefore, it is widely used to solve multi-objective problems in power systems. The swarm incorporates numerous particles. Every one of them presents a candidate solution, i.e. each of them is usually a scalar vector. As shown in the following equations, to achieve the required goals, the variables must be updated using search particles.

$$V_i^{k+1} = \omega \times V_i^k + C_1 \times rand_1(.) \times \left(P_{best,i}^k - X_i^k\right) + C_2 \times rand_2(.) \times \left(G_{best,i}^k - X_i^k\right) \qquad (65)$$

$$X_i^{k+1} = X_i^k + V_i^{k+1} \qquad (66)$$

where V_i^{k+1} is the updated velocity vector of the ith particle; $rand_1(.)$ and $rand_2(.)$ are arbitrary numbers restricted by [0, 1] values; X_i^{k+1} illustrates the updated position of the ith particle; ω, C_1, and C_2 are weight movement factors and learning factors, consequently.

5.2. The mathematical model:

In the proposed mathematical model for optimal operation, the variables are binary and continuous. The continuous variables such as the electrical energy swapped with the upstream network, the electrical power generated by the CCHP, the electrical power consumed by the electrolyzer, input electrical power to the SWD operation, the electrical power exchanged with the SPCAES, the electrical power transformed up/down, the output thermal power of AB, input thermal power to the AC, the thermal power swapped between the TESS and the thermal hub, the input electrical power to the ISC, the thermal power transferred up/down, at each hour. The binary variables are implemented to stop the consuming and generating modes of the storage from running at the same time. It should be noted that the Normal PDF is used for electrical, thermal, hydrogen, freshwater, and cooling demands, Beta PDF for PV, and Weibull PDF for WT which are considered in the model. The vector of decision variables is as shown.

$$f_b(si) = \begin{cases} \frac{\Gamma(\alpha_s+\beta_s)}{\Gamma(\alpha_s)\Gamma(\beta_s)} \times si^{(\alpha_s-1)} \times (1-si)^{(\beta_s-1)} & 0 \leq si \leq 1, \\ 0 & otherwise \end{cases} \quad \alpha_s \geq 0, \ \beta_s \geq 1 \tag{59}$$

$$\beta_s = (1-\mu_s) \times \left(\frac{\mu_s \times (1+\mu_s)}{\sigma_s^2} - 1\right) \tag{60}$$

$$\alpha_s = \frac{\mu_s \times \beta_s}{(1-\mu_s)} \tag{61}$$

6. Case study

6.1. test system settings and information

The scheduling horizon in this subsection is specified to be 96 hours. The total time horizon is then divided into 4 days by setting one hour as the calculation period. **Fig. 2** depicts the electrical and thermal loads per hour[26]. The electricity demand is high during the middle of the day during all seasons, but its maximum value is in the summer, while the demand for thermal energy during all seasons is at its maximum at the beginning and end of the day, and the maximum value it reaches between all seasons is in the winter. 400 EVs are supposed to be in this energy center. The charging energy of an electric vehicle is equal to its daily energy consumption. The uncoordinated charge load of EVs over the 96 hrs in addition to the hydrogen energy

and cooling demands are demonstrated in **Fig. 3**. As indicated the demand for cooling energy is high during the summer, while the winter does not witness any cooling loads. As for hydrogen loads and EV charging, they are equal over the four seasons. Water loads are also equal over the four seasons for a one-year time horizon [8] as displayed in **Fig. 4**. The forecasted electricity and gas prices for all seasons [26] are shown in **Fig. 5**. As demonstrated, the electricity market for each season changes hourly so that the market witnesses low prices in the first half of the day. However, prices rise to reach the peak in the second half of the day and after that, the general trend is downward. While the gas market includes one tariff for each season of the year. **Fig. 6** presents the characteristics of the PV and WT output power[26, 54]. The parameters of the EH component and other useful data are tabulated in **Table 2.**

$$\Upsilon(t) = \begin{bmatrix} P^{Grid}(t), P_e^{PGU}(t), H^{AB}(t), P_{c,d}^{CAES}(t), \\ P_{c,d}^{TESS}(t), P_{c,d}^{ISC}(t), P^{EL}(t), P^{RO}(t), P^{UP/DO}(t), H^{UP/DO}(t) \end{bmatrix} \tag{67}$$

Table 2. Parameters of the EH components [8, 26].

| Parameters of Grid and ESSs					
Parameter	**Value**	**Parameter**	**Value**	**Parameter**	**Value**
$P_{min}^E(kW)$	0.0	$P_{max\_c}^{ESS}(kW)$	470	η_d^{ESS}	0.95
$P_{max}^E(kW)$	3500	$P_{max\_d}^{ESS}(kW)$	180	K^{ISC}	0.90
η^{TR}	0.99	η_c^{ESS}	0.9	$\emptyset^{H,UP}$(cent/kWh)	0.1
$\emptyset^{H,DO}$(cent/kWh)	0.1	$\emptyset^{E,UP}$(cent/kWh)	0.1	$\emptyset^{E,UP}$(cent/kWh)	0.1
$MR^{E,UP}$	0.5	$MR^{E,DO}$	0.2	$MR^{H,UP}$	0.5
$MR^{H,DO}$	0.2				
Hydrogen devices and SWD parameters					
Parameter	**Value**	**Parameter**	**Value**	**Parameter**	**Value**
$SOC_{max}^{WST}(m^3)$	700	η^{EL}	0.75	$SOC_{max}^{H2S}(kW)$	40
$P_{max}^{EL}(kW)$	400	η^{FC}	0.5		
HHV^{h2}	39.7	SOC_0^{H2S}	4		
Emission coefficients		AC and HRU		EVs	
Parameter	**Value**	**Parameter**	**Value**	**Parameter**	**Value**
B_e (kg/kWh)	0.972	η^{HRU}	0.82	$EV_{capacity}$ (kWh)	40
B_g (kg/kWh)	0.23	K^{AC}	0.9	$EV_{initial\_SOC}$	20%
PGU		GB		EV_{max_SOC}	80%
η_e^{PGU}	0.42	**Parameter**	**Value**	E((¥/kg)	0.031
η_h^{PGU}	0.48	$H_{min}^{AB}(kW)$	0	p_{-ch} (kWh)	8
$P_{min}^{PGU}(kW)$	140	$H_{max}^{AB}(kW)$	2300		
$P_{max}^{PGU}(kW)$	1050	η_h^{AB}	0.9		
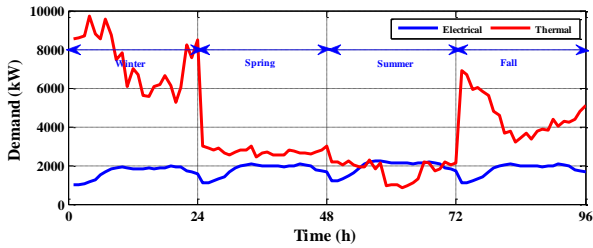
Fig 2. The electrical and thermal loads per hour.
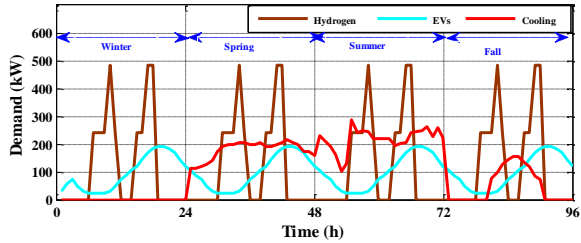

Fig 3. The EVs, hydrogen, and cooling demands per hour.
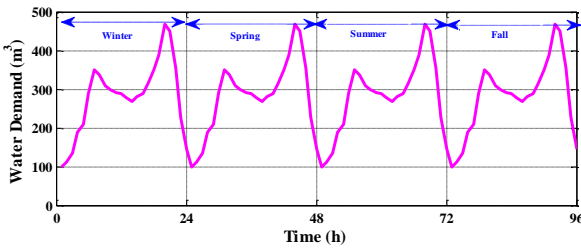

Fig 4. The water demand for a one-year time horizon.
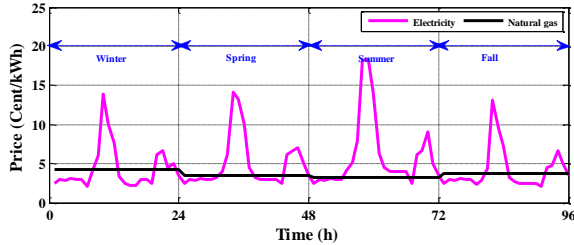

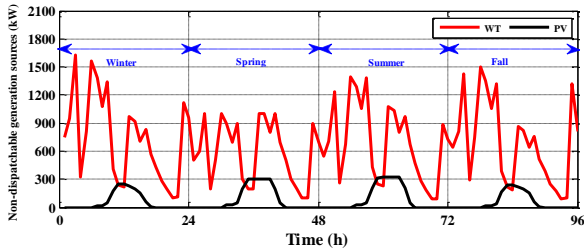**Fig 5.** The forecasted electricity and gas prices for all seasons.

Fig 6. The characteristics of the PV and WT output power.

6.2. Results and discussions:

The results of implementing electrical plus thermal DRP and EVs are discussed in this section. Four cases were considered for evaluating the effect of EV's coordinated charge mode and DRP considering water and hydrogen
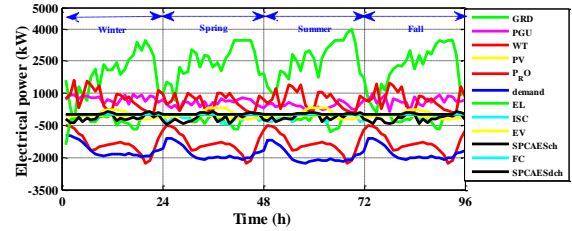
Fig 7. The electrical power balance of the studied EH components during the base case.
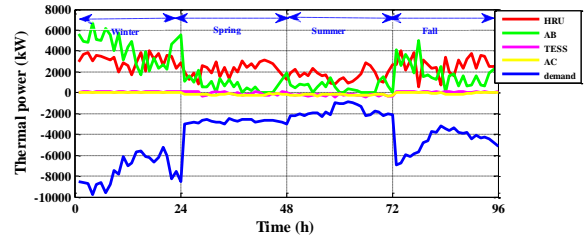
Fig 8. The thermal power dispatch under the base case.

system on the overall system cost as follows:

- Case 1: a basic case is taken into account with no DRP and uncoordinated EV charge mode.

- Case 2: electrical DRP and uncoordinated EV charge mode are considered in this case.

- Case 3: electrical and thermal DRP and uncoordinated EV charge mode are considered in this case.

- Case 4 (proposed): electrical and thermal DRP with coordinated EVs mode are considered.

1. The base case results:

The electrical power dispatch of the studied components of the EH, i.e. the CCHP unit, SPCAES, EVs, hydrogen system, and water system is provided in **Fig. 7**. As can be seen, the CCHP unit was operated during the winter and fall seasons since the thermal load is highest in the winter and fall seasons so the CCHP works to supply thermal energy in addition to the electrical energy. The SPCAES also assists the EH by charging during off-peak energy market hours, for example in the winter season, charging at times such as t = 1–8, 13–19, and 23, and discharging during peak hours such as 9–12, 20–22, and 24. The scheduling of EVs depends on their arrival and departure times, and the energy market does not influence EVs significantly. The energy market does not affect the water system because the amount of electrical energy withdrawn from the EH to produce water depends on the amount of water required per hour. As for the hydrogen

system, H2S discharges during high electricity price hours to reduce the electrical energy drawn by the electrolyzer at these times to meet the hydrogen loads.

The results of thermal energy distribution under the base case are shown in **Fig. 8**. Since CCHP produces electricity and thermal energy concurrently, it is obvious from the figure that it also produces thermal energy at peak times and the boiler produces thermal energy at high thermal load times to reach the required balance. The heat storage unit collaborates in getting the required balance under case 1; the redundant thermal energy produced by the thermal hub is used to charge the TESS during times of low thermal energy tariff as shown. Other than that, the TESS is unloading.

As **Fig. 9** shows, when there is a cooling load, both the AC and the ISC supply the cooling loads with the required energy. The ISC charges electricity during low electricity costs and discharges cooling energy during high electrical power prices.
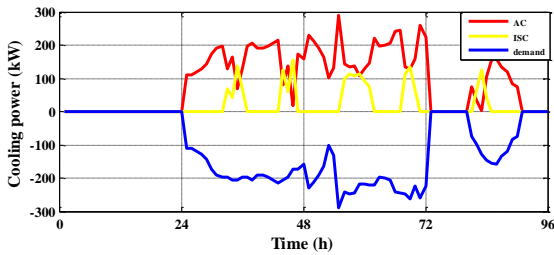
Fig 9. Dispatched cooling power during the base case.
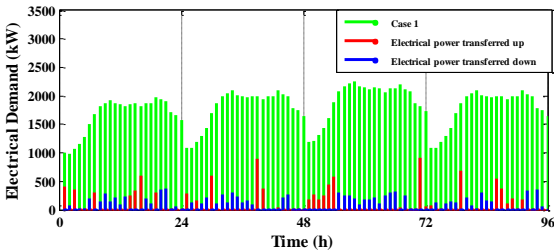
Fig 10. The amount of electrical energy transferred up/ down compared to the base case.
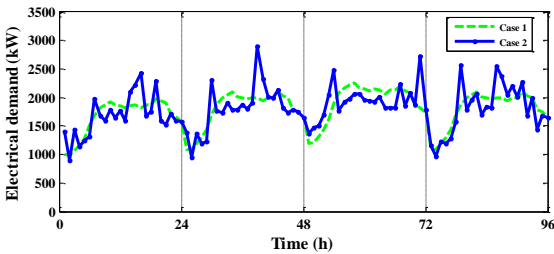

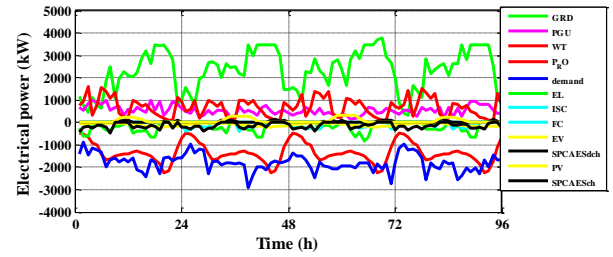**Fig 11.** The change in electrical load with implementing EDRP compared to the basic case.

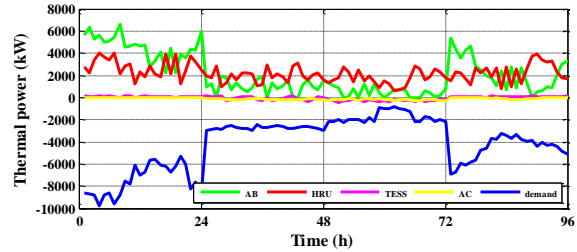**Fig 12.** The electrical power balance with implementing EDRP.

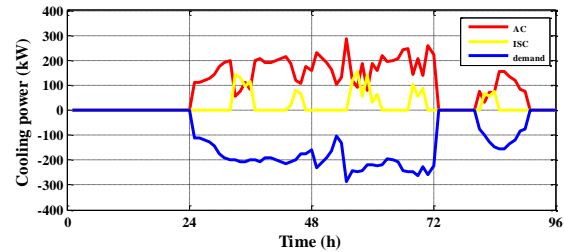**Fig 13.** The thermal power balance during case 2.

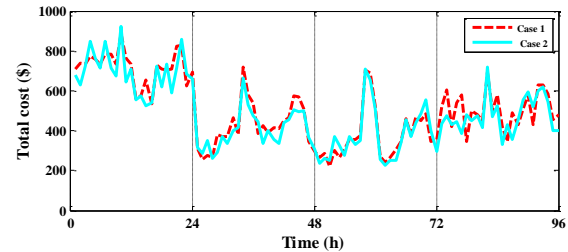**Fig 14.** The optimal cooling power dispatch in case 2.

Fig 15. The effect of applying EDRP on the total cost of the EH.

2.   Results of case 2:

Figs. 10 and 11 illustrate the effects of the EDRP on the electrical loads. To decrease the total costs of the EH, the customers reduce their load during peak hours in the energy market and shift it to off-peak hours for participating in the EDRP. For example, in **Fig. 10** in the winter season, loads are shifted from hours t = 6, 8–13, 17-18,20-23, in which energy prices are high, to other hours in which energy prices are low.

Fig. 12 shows the balance in electrical energy between production and consumption per hour in the case of applying EDRP. As shown in the figure, the electrical

load differs from the base case as a consequence of shifting the electrical load from peak hours to off-peak. Therefore, the electrical energy produced by the PGU increases during times of low electricity price hours compared to the base case due to the increased load during these times. For instance, the power produced by the PGU increases during times 25-28, 37, 47-48 and decreases during the rest of the day. As for the SPCAES, due to the increased load during off-peak hours, the charge of the SPCAES decreases during times of off-peak compared to the base case. For example, in the spring season, at the following times: 25-28 30-32 37 40-41 48 the charge of the SPCAES decreases. Likewise, for ISC, the value of the electrical energy consumed for charging it during times of off-peak is lower in the second case than in the first case. For instance, in the spring season, at times 31-32,38-43, and 47, the value of the ISC charging power decreases in the second case compared to the first case.

As we mentioned in the previous paragraph, the production of CCHP from electrical energy decreases in times of high electricity prices. Therefore, the production of CCHP from thermal energy also decreases at these times. For example, in the winter season, the thermal production of the HRU decreases in periods 9-12 and 20-21, which are peak hours, and increases in the following times 4-7 13 19 22-23 which are off peak hours. As a result, the production of thermal energy by the AB increases during the periods 9-12 and 20-21 to reach the required thermal balance, as well as for the rest of the seasons. As shown in **Fig. 13**.

The optimal cooling power dispatch in case 2 is represented in **Fig. 14**. As indicated as a result of the decrease in electrical energy consumed to charge the ISC, the cooling energy discharged is correspondingly reduced Therefore, the cooling energy produced by AC increases to reach the required balance in cooling energy. **Fig. 15**. shows the effect of applying EDRP on the total cost of the EH. The results show that the EDRP reduces the total costs by 4.0% compared to the basic case with total electrical power transferred up for each day equals the total electrical power transferred down for the same period.
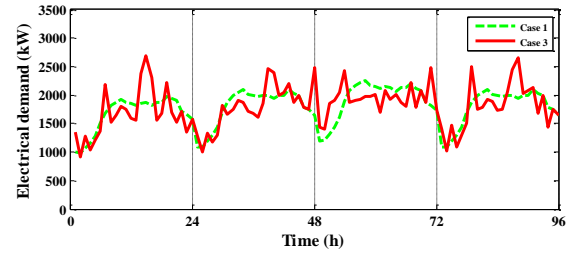

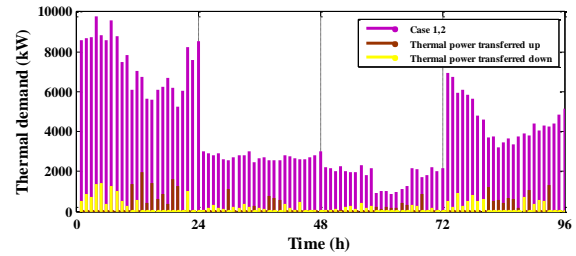**Fig 16.** The electrical demand of case 3 compared to the base case.

Fig 17. The thermal power transferred up/ down with implementing HDRP.
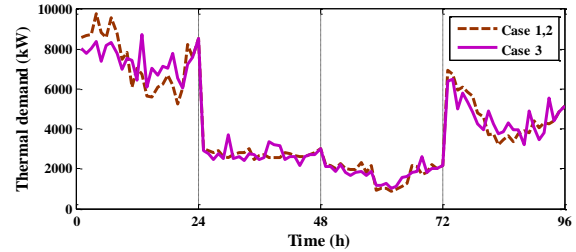

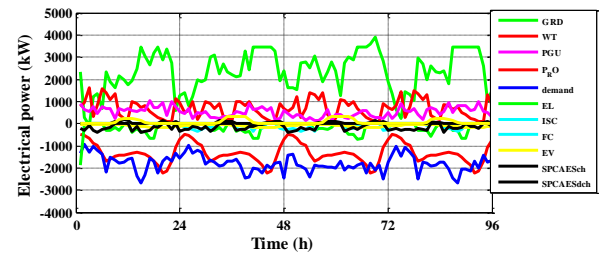**Fig 18.** the final form of the thermal load in the third case compared to the base case.

Fig 19. The electrical power balance in case 3.
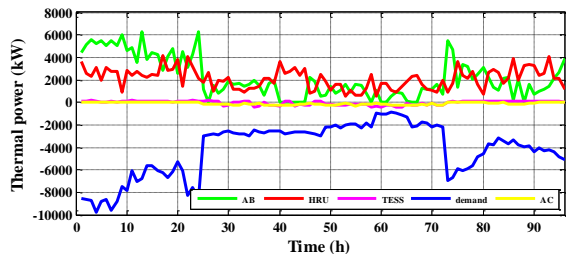

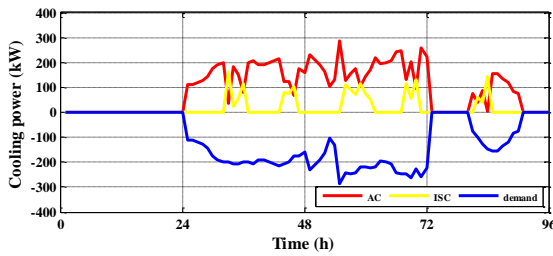**Fig 20.** The thermal power balance in case 3.

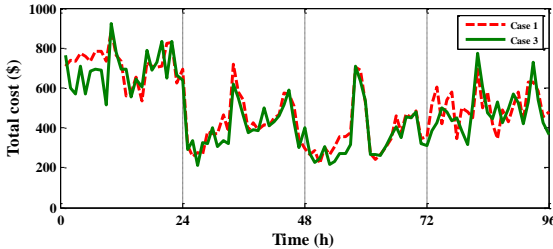**Fig 21.** The cooling power balance in case 3.

Fig 22. The effect of applying EDRP and HDRP on the total cost of the EH.

3.   Results of case 3:

Fig. 16. Declares the electrical demand by applying electrical and thermal DRP compared to the base case. As mentioned in the second case about the effect of adding EDRP on the electrical load, the same thing happens to the electrical load in the third case. As for the shape of the heat load with the addition of HDRP, **Fig. 17**. Shows the times when there is an increase or decrease in thermal energy. As shown, during times of high thermal load, the HDRP reduces the loads and adds these loads at non-peak times. For example, in the fall season, the heat load decreases at times 73-80, 87-88, and 90-92, which are peak times, and increases during the rest of the times during non-peak times. **Fig. 18**. Shows the final form of the thermal load in the third case and also explains the difference between it and the basic case.

Regarding electrical balance, it is exactly as mentioned in the previous case, as shown in **Fig. 19**. As for the thermal balance illustrated in **Fig. 20**. Due to the decrease in thermal loads at peak times, the thermal energy produced by the AB decreases at the same times. For example, the thermal energy produced by the AB decreases at the following times 1-8 and 22, which are considered peak times during a winter day. Therefore, the energy consumed through the AC increases during peak times.

Due to the increase in the thermal energy consumed by AC, the cooling energy generated from it increases accordingly, and this helps in reaching the required balance in cooling energy as a result of the decrease in the

charging and discharging energy of the ISC which is due to implementing EDRP as shown in **Fig. 21**. Which shows the optimal dispatch of cooling energy in case 3. As a result, the total cost in the third case is significantly lower than the first case by 4.8%, as observed in **Fig. 22**.
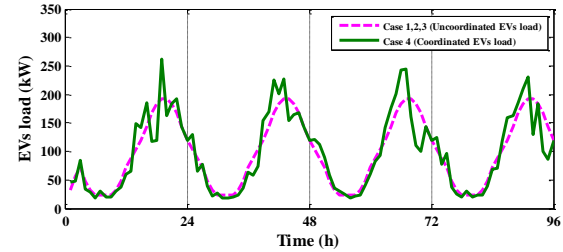

Fig 23. the difference in the EVs load pattern between coordinated and uncoordinated modes.
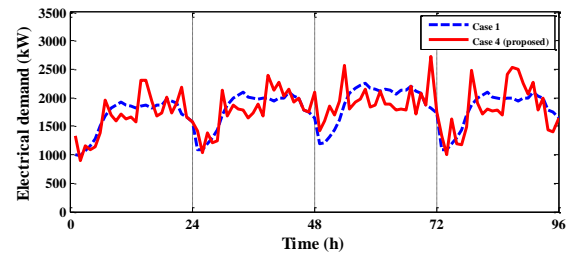

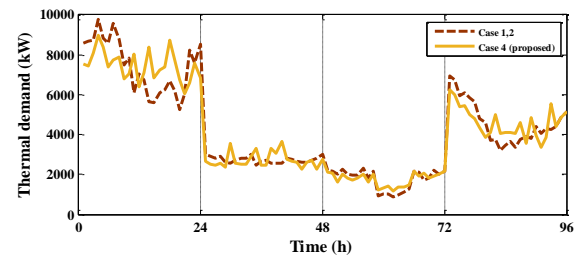**Fig 24.** The electrical demand of the proposed method compared to the base case.

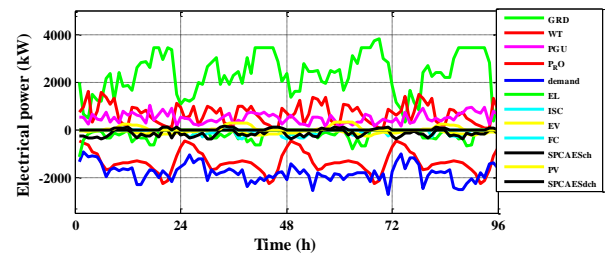**Fig 25.** The thermal demand of the proposed method compared to the base case.

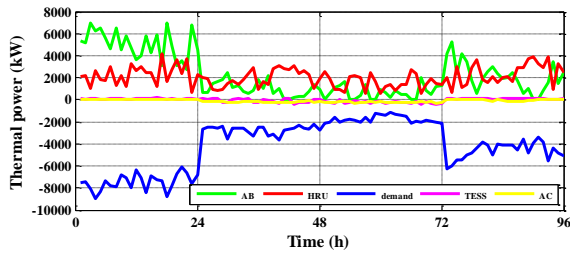**Fig 26.** The electrical power balance through the proposed method.

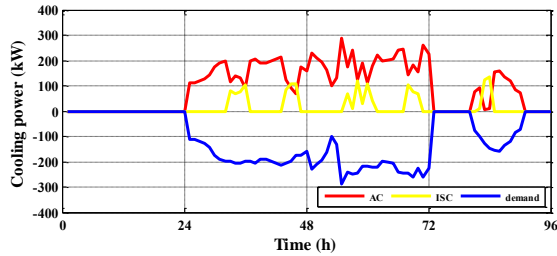**Fig 27.** The thermal power balance through the proposed method.

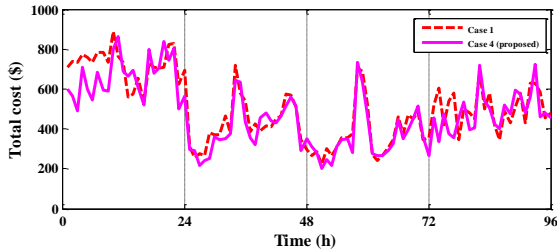**Fig 28.** The cooling power balance through the proposed method.

Fig 29. The total cost of the proposed method compared to the base case.

4. Results of case 4:

In this case, the EVs are charged in a coordinated mode, which is a price-based mode for charging the EVs the difference in the EVs load pattern between coordinated and uncoordinated modes is declared in **Fig. 23**. As for the electrical and thermal demand, as mentioned in Cases

2 and 3 about the effect of the EDRP on the shape of the electrical demand, it changes in the same way in Case 4. Likewise, the thermal load in the fourth case changes in the same manner as was mentioned in the third case, as shown in **Figs. 24** and **25**.

Fig. 26. Represents the optimal dispatch of electrical power by applying EDRP, HDRP, and coordinated EVs. As shown, the EVs charging power in this case decreases during times of high electricity price hours and increases during times of low electricity price hours. Therefore, the charge of ISC decreases accordingly, and the amount of electrical energy produced by the PGU during times of peak also decreases. It is clear from **Fig. 27**, which shows the shape of the thermal balance in case 4, that changing the charging mode of the EVs does not have a noticeable effect on the shape of the thermal balance in the third case. Due to the decrease in the charging energy of the ISC, consequently, the discharging energy of the ISC also decreases. To maintain the balance in cooling energy between generation and consumption, the cooling energy generated by the AC increases as represented in **Fig. 28**. The total cost and the difference in the total cost between the basic case and the proposed case per hour are illustrated in **Fig. 29**. The results show that with applying electrical and thermal DRP with coordinated charge mode of EVs the total costs are reduced by 6.3% compared to the basic case with total electrical, thermal power transferred up for the 24 hours equal the total electrical, and thermal power transferred down for the same period. The total EVs load throughout the day is also equal to the uncoordinated state. The comparison of the costs of different cases is represented in **Table 3. Fig. 30** Illustrates the difference between the total cost for the four cases and the cost reduction percentage for the four cases as well.

Table 3. The comparison of the costs of different cases.

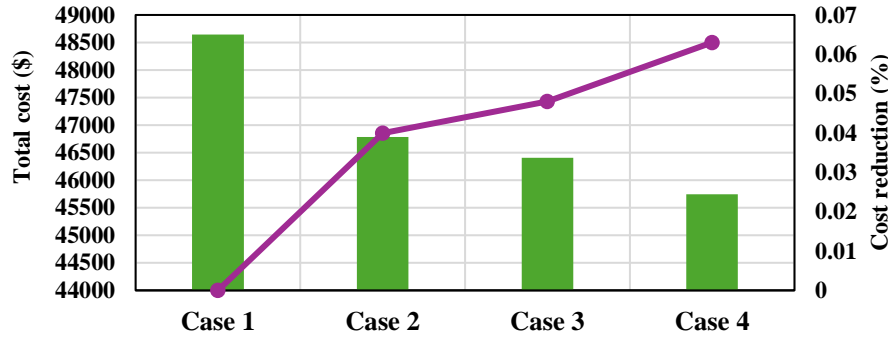|	Electrical cost	Gas cost	Emission cost	Discomfort Cost	Total cost	Cost reduction (%)
Case 1	11537.2	35144.7	1961.2	--	48643.1	--
Case 2	11355.2	33476.6	1931.4	20.2	46783.5	4.0%
Case 3	11424.9	32983.5	1932.6	67.4	46408.3	4.8%
Case 4	11334.7	32412.4	1921.6	77.6	45746.3	6.3%

Fig 30. The total cost and the cost reduction percentage for the four cases.

5. Comparison with an existing work

To illustrate the superiority of the proposed work implemented in this paper, it is compared with other similar research on the same point such as [4]. Therefore, by comparing the results of implementing electrical and thermal DRP with managed EV charging mode for both papers, it is concluded that by implementing electrical and thermal DRP with EVs managed charging mode, the total cost of this system for one day is reduced by 9.1% while in the existing work, the total cost is reduced by 5.33%. As for the operation cost, it improved by approximately 9.56% while in the previous research, it was reduced by .35%. Taking into account that this research paper includes SWD operation, which represents an additional electrical load that has not been taken into account in existing work. This paper also includes a hydrogen system which is not considered in existing work.

7 Conclusion

At present, EH is one of the traditional and effective complementary systems through which the increasing energy demand is met by integrating different energy sources, especially renewable energy sources, due to their advantages of reducing carbon emissions in addition to other benefits gained from implementing RES. In this paper, the optimal operation of a comprehensive EH system including a CCHP unit, auxiliary boiler, SPCAES, ISC, TESS, hydrogen system, SWD system, PV arrays, and WT. The EVs are also considered to study the demand for EV charging loads under coordinated and uncoordinated charging modes which formulates a fundamental contribution of this study, taking into account the behaviors and interactions of EV owners. Considering the undeniable role of demand response programs (DRPs) as a suitable alternative to fix load curves and increase system efficiency. Therefore Developing prosperous optimal transactions of EHs by applying thermal and electrical DRP under different EV charging procedures is the main purpose of this study as this optimization aims to deal with both economic and environmental issues. For assessing the behavior of the system considered, four cases were evaluated, including unmanaged/managed EV charging, with and without DR methods. Numerical results show that applying EDRP on the studied system with unmanaged EV charging mode can reduce the operational costs by 4.08%, achieving a 1.54% reduction in emission cost as well. These results revealed that the minimization of operation and emission costs in Case 2 has led to a decrease in overall costs by approximately 4% compared to the basic case without any DRP. The results also showed that by applying thermal and electrical DRPs on the basic model with uncoordinated EV charging mode, the total cost can be decreased by 4.8% with a 5% reduction in operational costs and a 1.48% reduction in emission costs. Notably, Case 4, which encompassed both electrical and thermal DRP and coordinated EV charging mode, presented the most auspicious outcomes. It achieved a 6.3 % reduction in total cost.   Achieving a 6.51 % reduction in operational costs, furthermore, a 2.06 % reduction in emission costs is achieved. From this, it was concluded that better economic and environmental conditions of EH can be achieved by applying thermal and electrical DRP with a managed EV charging mode.

Appendix

Symbol	Description	Symbol	Description
Index		U^{RO}	1 if RO is on at time t; otherwise 0.
T	Set of hours in the operation period.	v_{ci}	Cut-in wind speed (m/s).
Parameters		v_{co}	Cut-out wind speed (m/s).
$C^{AC}(t)$	The cooling power generated from the AC at time t (kW).	v_r	Rated wind speed (m/s).
$C_{ce}(t)$	Carbon emission cost at hour t($) .	$W^{RO}(t)$	The water generated by the SWD-RO at time t (m^3).
$\boldsymbol{C_e(t)}$	The net electricity purchasing cost at time t ($).	W^{RO-max}	`The limit of the power generated by the SWD unit.
C_{EDRP}	Discomfort cost resulting from implementing the EDRP	$W^{wd}(t)$	The water demand of the EH at time t (m^3).
C_{HDRP}	Discomfort cost resulting from implementing the HDRP	$\rho_e(t)$	Sell and purchase Electricity price at time t ($/kWh).
$C_g(t)$	The net gas purchasing cost at time t ($).	η_d^{SPCAES}	The discharging efficiency of the SPCAES.
$CL(t)$	The cooling demand of the EH at time t (kW).	$\eta_{ch,i}$	The charging efficiency of the EV i.
$D^{h2}(t)$	The hydrogen demand of the EH at time t (kW)	$\eta_{d,i}$	The discharging efficiency of the EV i.
$E^{ESS}(t)$	Energy remaining in the ESS at hour t (kWh).	η_c^{ESS}	The charging efficiency of the ESS.
E_{min}^{ESS}	Minimum energy in ESS (kWh).	η_d^{ESS}	The discharging efficiency of the ESS.
E_{max}^{ESS}	Maximum energy in ESS (kWh).	η^{EL}	The electrolyser efficiency.
$H^{AC}(t)$	Heating power consumed by AC at hour t (kW).	η^{FC}	The fuel cell efficiency.
H_{min}^{AC}	Minimum heating power consumed by AC at hour t (kW).	η_h^{GB}	The heat generation efficiency of the AB.
H_{max}^{AC}	Maximum heating power consumed by AC at hour t (kW).	η_e^{PGU}	The electrical generation efficiency of the PGU.
$H^{AB}(t)$	Heating power generated by AB at hour t (kW).	η_h^{PGU}	The heat generation efficiency of the PGU.
H_{min}^{AB}	Minimum heating power generated by AB at hour t (kW).	η^{HRU}	The HRU efficiency.
H_{max}^{AB}	Maximum heating power generated by AB at hour t (kW).	η^{pv}	The efficiency of the PV module.
$H^{HRU}(t)$	The co-product heat generated by PGU at hour t (kW).	η^{sol}	The efficiency of the PV module.
H_{min}^{HRU}	Minimum heating power generated by HRU at hour t (kW).	η_t	Transformer efficiency.
H_{max}^{HRU}	Maximum heating power generated by HRU at time t (kW).	$f_b(si)$	Beta PDF of si.
$H^{UP}(t)$ /$H^{DO}(t)$	thermal power transferred up and down by the DR program at time t	$\emptyset^{E,UP}/\emptyset^{E,DO}$	Costs of Increasing and decreasing the electrical load by implementing the DRP.
$HL(t)$	Heating demand at time t (kW).	$\emptyset^{H,UP}/\emptyset^{H,DO}$	Costs of Increment and decrement the thermal load by implementing the DRP.
$H2^{im}(t)$	The imported hydrogen power to hydrogen storage at time t (kW).	θ	Carbon dioxide processing cost ($/kg).
$H2^{ex}(t)$	The exported hydrogen power from hydrogen storage at time t (kW).	Φ_e	Equivalent emission coefficients for electricity (kg/kWh).
K^{AC}	Performance coefficient of AC.	Φ_g	Equivalent emission coefficients for gas (kg/kWh).
K^{ISC}	Performance coefficient of ISC.	$\rho_g(t)$	Gas price at time t ($/kWh).
$MR^{E,UP}$ /$MR^{E,DO}$	Maximum increment and decrement ratio for the electrical requirements.	μ_d	Mean of forecasted demands (kW/m2).
$MR^{H,UP}$ /$MR^{H,DO}$	Maximum increment and decrement ratio for the thermal requirements.	μ_s	Mean of forecasted solar irradiance (kW/m2).
NO_t	The number of EVS connected to the grid at the time (t).	$f_d(l)$	Normal PDF of l.
$P^{EL}(t)$	The electrical power consumed by the electrolyzer at time t (kW).	α_s	Parameter of the Beta PDF.
P^{EL-max}	Maximum imported power limit by the electrolyzer at time t (kW).	β_s	Parameter of the Beta PDF.
$P^{FC}(t)$	The electrical power generated from the fuel cell at time t (kW).	σ_d	Standard deviation of forecasted demands (kW/m2).
$P^{fc}(t)$	The hydrogen power consumed by the fuel cell at time t (kW).	σ_d	Standard deviation of forecasted demands (kW/m2).
$P_C^{ISC}(t)$	The charging power of the ISC at time t (kW).	σ_s	Standard deviation of forecasted solar irradiance (kW/m2).
$P_d^{ISC}(t)$	The discharged power of the ISC at time t (kW).	Δt	Time interval (one hour).
$P^{RO}(t)$	The electrical power consumed by the SWD-RO at time	$f_w(v)$	Weibull PDF of v.

	t (kW)		
$P_c^{SPCAES}(t)$	The charging power of the SPCAES at time t (kW).	**Abbreviations**	
$P_d^{SPCAES}(t)$	The discharged power of the SPCAES at time t (kW).	AB	Auxiliary boiler.
P_g^{SPCAES}	The value of gas entering the SPCAES (kW).	AC	Absorption chiller.
$P^{UP}(t)$ $/P^{DO}(t)$	electric power transferred up and down by the DR program at time t	CAES	Compressed air energy storage.
$P_{ch,i,t}(t)$	The charging power of EVS at time t (kW).	CHP	Combined heating and power unit.
$P_{ch,,max}(t)$	The charging capacity of each EV at time t (kW).	CCHP	Combined cooling, heat, and power.
$P_{d,i,t}(t)$	The discharging power of EVS at time t (kW).	DRP	Demand response program.
$P^E(t)$	Real power exchanged from the upstream grid after transformer at time t (kW)	EDRP	Electrical demand response program.
P_{min}^E	Minimum Real power exchanged from the upstream grid after transformer at time t (kW)	EH	Energy-hub.
P_{max}^E	Maximum Real power exchanged from the upstream grid after transformer at time t (kW)	ESS	Energy storage systems.
$P_c^{ESS}(t)$	The charging power of ESS at time t (kW).	EVs	Electric vehicles.
$P_d^{ESS}(t)$	The discharged power of ESS at time t (kW).	FC	Fuel cell.
P_{c-max}^{ESS}	The maximum charged power of ESS at time t (kW).	GA	Genetic algorithm.
P_{d-max}^{ESS}	The maximum discharged power of ESS at time t (kW).	HDRP	Heat demand response program.
$P^{EV}(t)$	The power of the EVs at time t (kW).	HRU	Heat recovery unit.
P_g^{AB}	The value of gas entering the AB (kW).	H2S	Hydrogen storage.
P_g^{PGU}	The value of gas entering the PGU (kW).	ISC	Ice storage conditioner.
$P_e^{PGU}(t)$	The electrical power generated from the PGU at time t (kW).	MG	Microgrid.
P_{min}^{PGU}	The minimum electrical power generated from PGU at time t (kW).	MILP	Mixed integer linear programming.
P_{max}^{PGU}	The maximum electrical power generated from PGU at time t (kW).	NG	Natural gas.
$P^{Grid}(t)$	The real power exchanged with the upstream grid at time t (kW).	PDF	Probability distribution function.
P_{gas}	The value of the net gas entering the EH (kW).	PEVs	Plug-in EVs.
$P_c^{TESS}(t)$	The charged power of the TESS at time t (kW).	PGU	Power generation unit.
$P_d^{TESS}(t)$	The discharged power of the TESS at time t (kW).	PSO	Particle swarm optimizer.
$PL(t)$	The electrical demand of the EH at time t (kW).	PV	Solar photovoltaic.
$P^{PV}(t)$	The output power of the PV modules at time t (kW).	RES	Renewable energy resources.
p_{rated}	The rated power generated from the WT at time t (kW).	RMILP	Robust mixed integer linear programming.
$P^{WT}(t)$	The output power of the WT at time t (kW).	RO	Reverse osmosis technology.
SEC^{RO}	The SWD performance coefficient (kW/m^3)	SOC	State of charge.
si	Solar irradiance (kW/m^2)	SPCAES	Solar-powered compressed air energy storage.
$SOC_{i,t}$	State of charge of the EV i at time t.	SWD	Sea water desalination.
$SOC^{H2S}(t)$	State of charge of the HS at time t (kg)	TESS	Thermal energy storage system.
$SOC^{H2S-max}$	The maximum SOC of the HS.	WST	Water storage tank.
s^{pv}	Area of PV module (m2).	WT	Wind turbine.
s^{sol}	Area of PV module (m2).		
u	Charging status of EVs at hour t (1 for charging mode; otherwise, 0).		
$U^{ESS}(t)$	Charging status of ESS at hour t (1 for charging mode; otherwise, 0).		
U_C^{H2S}	Charging status of HS at hour t (1 for charging mode; otherwise 0).		

References

[1] J. Lian, Y. Zhang, C. Ma, Y. Yang, and E. Chaima, "A review on recent sizing methodologies of hybrid renewable energy systems," *Energy Conversion and Management,* vol. 199, p. 112027, 2019.

[2] K. Saidi, M. M. Rahman, and M. Amamri, "The causal nexus between economic growth and energy consumption: New evidence from global panel of 53 countries," *Sustainable cities and society,* vol. 33, pp. 45-56, 2017.

[3] S. Eslami, A. Gholami, A. Bakhtiari, M. Zandi, and Y. Noorollahi, "Experimental investigation of a multi-generation energy system for a nearly zero-energy park: A solution toward sustainable future," *Energy Conversion and Management,* vol. 200, p. 112107, 2019.

[4] M. Aslani, M. Mashayekhi, H. Hashemi-Dezaki, and A. Ketabi, "Robust optimal operation of energy hub incorporating integrated thermal and electrical demand response programs under various electric vehicle charging modes," *Applied Energy,* vol. 321, p. 119344, 2022.

[5] M. Rawa, Y. Al-Turki, K. Sedraoui, S. Dadfar, and M. Khaki, "Optimal operation and stochastic scheduling of renewable energy of a microgrid with optimal sizing of battery energy storage considering cost reduction," *Journal of Energy Storage,* vol. 59, p. 106475, 2023.

[6] M. Roustai, M. Rayati, A. Sheikhi, and A. Ranjbar, "A scenario-based optimization of smart energy hub operation in a stochastic environment using conditional-value-at-risk," *Sustainable cities and society,* vol. 39, pp. 309-316, 2018.

[7] M. Duan, A. Darvishan, R. Mohammaditab, K. Wakil, and O. Abedinia, "A novel hybrid prediction model for aggregated loads of buildings by considering the electric vehicles," *Sustainable cities and society,* vol. 41, pp. 205-219, 2018.

[8] R. Li and S. SaeidNahaei, "Optimal operation of energy hubs integrated with electric vehicles, load management, combined heat and power unit and renewable energy sources," *Journal of Energy Storage,* vol. 48, p. 103822, 2022.

[9] A. Merabet, A. Al-Durra, T. El Fouly, and E. F. El-Saadany, "Multifunctional energy management system for optimized network of microgrids considering battery degradation and load adjustment," *Journal of Energy Storage,* vol. 100, p. 113709, 2024.

[10] O. Abedinia, M. Lu, and M. Bagheri, "An improved multicriteria optimization method for solving the electric vehicles planning issue in smart grids via green energy sources," *IEEE Access,* vol. 8, pp. 3465-3481, 2019.

[11] S. Maghsoodi, V. Talavat, and S. Galvani, "Probabilistic scheduling of a comprehensive energy hub integrated with renewable energy sources considering the correlation between uncertain variables," *Sustainable Energy, Grids and Networks,* vol. 36, p. 101222, 2023.

[12] Y. Chen, M. Tian, J. Xue, L. Zhang, and J. Ying, "Data-driven approaches to achieve energy transition: Statistical analysis of demand-side management and smart decision making in urban energy hub networks," *Sustainable Cities and Society,* vol. 101, p. 105150, 2024.

[13] A. Hussain, S. M. Arif, M. Aslam, and S. D. A. Shah, "Optimal siting and sizing of tri-generation equipment for developing an autonomous community microgrid considering uncertainties," *Sustainable Cities and Society,* vol. 32, pp. 318-330, 2017.

[14] F. Jamalzadeh, A. H. Mirzahosseini, F. Faghihi, and M. Panahi, "Optimal operation of energy hub system using hybrid stochastic-interval optimization approach," *Sustainable Cities and Society,* vol. 54, p. 101998, 2020.

[15] P. Emrani-Rahaghi and H. Hashemi-Dezaki, "Optimal scenario-based operation and scheduling of residential energy hubs including plug-in hybrid electric vehicle and heat storage system considering the uncertainties of electricity price and renewable distributed generations," *Journal of Energy Storage,* vol. 33, p. 102038, 2021.

[16] X. Wang, Y. Liu, C. Liu, and J. Liu, "Coordinating energy management for multiple energy hubs: From a transaction perspective," *International Journal of Electrical Power & Energy Systems,* vol. 121, p. 106060, 2020.

[17] Y. Allahvirdizadeh, S. Galvani, and H. Shayanfar, "Data clustering based probabilistic optimal scheduling of an energy hub considering risk-averse," *International Journal of Electrical Power & Energy Systems,* vol. 128, p. 106774, 2021.

[18] A. A. Eladl, M. I. El-Afifi, M. A. Saeed, and M. M. El-Saadawi, "Optimal operation of energy hubs integrated with renewable energy sources and storage devices considering CO2 emissions," *International Journal of Electrical Power & Energy Systems,* vol. 117, p. 105719, 2020.

[19] M. Vahid-Pakdel, S. Nojavan, B. Mohammadi-Ivatloo, and K. Zare, "Stochastic optimization of energy hub operation with consideration of thermal energy market and demand response," *energy Conversion and Management,* vol. 145, pp. 117-128, 2017.

[20] S. Zeynali, N. Rostami, A. Ahmadian, and A. Elkamel, "Robust multi-objective thermal and electrical energy hub management integrating hybrid battery-compressed air energy storage systems and plug-in-electric-vehicle-based demand response," *Journal of Energy Storage,* vol. 35, p. 102265, 2021.

[21] R. Bahmani, H. Karimi, and S. Jadid, "Cooperative energy management of multi-energy hub systems considering demand response programs and ice storage," *International Journal of Electrical Power & Energy Systems,* vol. 130, p. 106904, 2021.

[22] M. Jadidbonab, E. Babaei, and B. Mohammadi-ivatloo, "CVaR-constrained scheduling strategy for smart multi carrier energy hub considering demand response and compressed air energy storage," *Energy,* vol. 174, pp. 1238-1250, 2019.

[23] S. Pazouki, M.-R. Haghifam, and A. Moser, "Uncertainty modeling in optimal operation of energy hub in presence of wind, storage and demand response," *International Journal of Electrical Power & Energy Systems,* vol. 61, pp. 335-345, 2014.

[24] A. Shabanpour-Haghighi and A. R. Seifi, "Simultaneous integrated optimal energy flow of electricity, gas, and heat," *Energy conversion and management,* vol. 101, pp. 579-591, 2015.

[25] T. Liu, D. Zhang, S. Wang, and T. Wu, "Standardized modelling and economic optimization of multi-carrier energy systems considering energy storage and demand response," *Energy conversion and management,* vol. 182, pp. 126-142, 2019.

[26] M. Jalili, M. Sedighizadeh, and A. S. Fini, "Stochastic optimal operation of a microgrid based on energy hub including a solar-powered compressed air energy storage system and an ice storage conditioner," *Journal of energy storage,* vol. 33, p. 102089, 2021.

[27] A. Heidari, S. Mortazavi, and R. Bansal, "Stochastic effects of ice storage on improvement of an energy hub optimal operation including demand response and renewable energies," *Applied Energy,* vol. 261, p. 114393, 2020.

[28] S. Nojavan, K. Saberi, and K. Zare, "Risk-based performance of combined cooling, heating and power (CCHP) integrated with renewable energies using information gap decision theory," *Applied Thermal Engineering,* vol. 159, p. 113875, 2019.

[29] J. Soares, M. A. F. Ghazvini, N. Borges, and Z. Vale, "A stochastic model for energy resources management considering demand response in smart grids," *Electric Power Systems Research,* vol. 143, pp. 599-610, 2017.

[30] C. Li *et al.*, "Energy hub-based optimal planning framework for user-level integrated energy systems: Considering synergistic effects under multiple uncertainties," *Applied Energy,* vol. 307, p. 118099, 2022.

[31] Z. Ma, Y. Zheng, C. Mu, T. Ding, and H. Zang, "Optimal trading strategy for integrated energy company based on integrated demand response considering load classifications," *International Journal of Electrical Power & Energy Systems,* vol. 128, p. 106673, 2021.

[32] X. Lu, Z. Liu, L. Ma, L. Wang, K. Zhou, and S. Yang, "A robust optimization approach for coordinated operation of multiple energy hubs," *Energy,* vol. 197, p. 117171, 2020.

[33] H. Kouchaki-Penchah *et al.*, "The role of hydrogen in a net-zero emission economy under alternative policy scenarios,"

International Journal of Hydrogen Energy, vol. 49, pp. 173-187, 2024.

[34] O. F. Noyan, M. M. Hasan, and N. Pala, "A global review of the hydrogen energy eco-system," *Energies,* vol. 16, no. 3, p. 1484, 2023.

[35] A. Mansour-Saatloo, M. Agabalaye-Rahvar, M. A. Mirzaei, B. Mohammadi-Ivatloo, M. Abapour, and K. Zare, "Robust scheduling of hydrogen based smart micro energy hub with integrated demand response," *Journal of Cleaner Production,* vol. 267, p. 122041, 2020.

[36] W. He, Y. Wang, and M. H. Shaheed, "Stand-alone seawater RO (reverse osmosis) desalination powered by PV (photovoltaic) and PRO (pressure retarded osmosis)," *Energy,* vol. 86, pp. 423-435, 2015.

[37] E. Koutroulis and D. Kolokotsa, "Design optimization of desalination systems power-supplied by PV and W/G energy sources," *Desalination,* vol. 258, no. 1-3, pp. 171-181, 2010.

[38] B. Zhou, B. Liu, D. Yang, J. Cao, and T. Littler, "Multi-objective optimal operation of coastal hydro-electrical energy system with seawater reverse osmosis desalination based on constrained NSGA-III," *Energy conversion and management,* vol. 207, p. 112533, 2020.

[39] M. W. Shahzad, M. Burhan, and K. C. Ng, "Pushing desalination recovery to the maximum limit: Membrane and thermal processes integration," *Desalination,* vol. 416, pp. 54-64, 2017.

[40] J. A. Aguilar-Jiménez, N. Velázquez, R. Beltrán, L. Hernández-Callejo, R. López-Zavala, and E. González-San Pedro, "Potential for thermal water desalination using microgrid and solar thermal field energy surpluses in an isolated community," in *Smart Cities: Second Ibero-American Congress, ICSC-CITIES 2019, Soria, Spain, October 7–9, 2019, Revised Selected Papers 2,* 2020: Springer, pp. 162-175.

[41] X. Luo, Y. Zhu, J. Liu, and Y. Liu, "Design and analysis of a combined desalination and standalone CCHP (combined cooling heating and power) system integrating solar energy based on a bi-level optimization model," *Sustainable Cities and Society,* vol. 43, pp. 166-175, 2018.

[42] A. Zidan, H. A. Gabbar, and A. Eldessouky, "Optimal planning of combined heat and power systems within microgrids," *Energy,* vol. 93, pp. 235-244, 2015.

[43] T. Ma, J. Wu, and L. Hao, "Energy flow modeling and optimal operation analysis of the micro energy grid based on energy hub," *Energy conversion and management,* vol. 133, pp. 292-306, 2017.

[44] X. Lu, K. Zhou, S. Yang, and H. Liu, "Multi-objective optimal load dispatch of microgrid with stochastic access of electric vehicles," *Journal of cleaner production,* vol. 195, pp. 187-199, 2018.

[45] N. H. Jabarullah, M. S. Shabbir, M. Abbas, A. F. Siddiqi, and S. Berti, "Using random inquiry optimization method for provision of heat and cooling demand in hub systems for smart buildings," *Sustainable Cities and Society,* vol. 47, p. 101475, 2019.

[46] K. Saberi, H. Pashaei-Didani, R. Nourollahi, K. Zare, and S. Nojavan, "Optimal performance of CCHP based microgrid considering environmental issue in the presence of real time demand response," *Sustainable cities and society,* vol. 45, pp. 596-606, 2019.

[47] X. Lu, Z. Liu, L. Ma, L. Wang, K. Zhou, and N. Feng, "A robust optimization approach for optimal load dispatch of community energy hub," *Applied Energy,* vol. 259, p. 114195, 2020.

[48] A. Ahmarinejad, "A multi-objective optimization framework for dynamic planning of energy hub considering integrated demand response program," *Sustainable Cities and Society,* vol. 74, p. 103136, 2021.

[49] E. Mokaramian, H. Shayeghi, F. Sedaghati, and A. Safari, "Four-objective optimal scheduling of energy hub using a novel energy storage, considering reliability and risk indices," *Journal of Energy Storage,* vol. 40, p. 102731, 2021.

[50] M. Kafaei, D. Sedighizadeh, M. Sedighizadeh, and A. S. Fini, "An IGDT/Scenario based stochastic model for an energy hub considering hydrogen energy and electric vehicles: A case study

of Qeshm Island, Iran," *International Journal of Electrical Power & Energy Systems,* vol. 135, p. 107477, 2022.

[51] P. Paudyal and Z. Ni, "Smart home energy optimization with incentives compensation from inconvenience for shifting electric appliances," *International Journal of Electrical Power & Energy Systems,* vol. 109, pp. 652-660, 2019.

[52] M. Fleschutz, M. Bohlayer, M. Braun, G. Henze, and M. D. Murphy, "The effect of price-based demand response on carbon emissions in European electricity markets: The importance of adequate carbon prices," *Applied Energy,* vol. 295, p. 117040, 2021.

[53] Y. Astriani, G. Shafiullah, and F. Shahnia, "Incentive determination of a demand response program for microgrids," *Applied Energy,* vol. 292, p. 116624, 2021.

[54] M. M. Sani, H. M. Sani, M. Fowler, A. Elkamel, A. Noorpoor, and A. Ghasemi, "Optimal energy hub development to supply heating, cooling, electricity and freshwater for a coastal urban area taking into account economic and environmental factors," *Energy,* vol. 238, p. 121743, 2022.